Non-Gaussian approach for equivalent static wind loads from wind tunnel measurements

Wafaa Kassir, Christian Soize, Jean-Vivien Heck, Fabrice de Oliveira

Submitted to Wind and Structures, An International Journal, *Vol. Preprint, No. (2017) 1–20*
DOI: http://dx.doi.org/10.12989/was.2017.25.6.589

Non-Gaussian approach for equivalent static wind loads from wind tunnel measurements

Wafaa Kassir[1,2a], Christian Soize*[1], Jean-Vivien Heck[2b] and Fabrice De Oliveira[2c]

[1]*Université Paris-Est, Modélisation et Simulation Multi-Echelle, MSME UMR 8208 CNRS, 5 Bd Descartes, 77454 Marne-la-Vallée, France*
[2]*Centre Scientifique et Technique du Bâtiment (CSTB), 11 Rue Henri Picherit, 44300 Nantes, France*

Abstract. A novel probabilistic approach is presented for estimating the equivalent static wind loads that produce a static response of the structure, which is "equivalent" in a probabilistic sense, to the extreme dynamic responses due to the unsteady pressure random field induced by the wind. This approach has especially been developed for complex structures (such as stadium roofs) for which the unsteady pressure field is measured in a boundary layer wind tunnel with a turbulent incident flow. The proposed method deals with the non-Gaussian nature of the unsteady pressure random field and presents a model that yields a good representation of both the quasi-static part and the dynamical part of the structural responses. The proposed approach is experimentally validated with a relatively simple application and is then applied to a stadium roof structure for which experimental measurements of unsteady pressures have been performed in boundary layer wind tunnel.

Keywords: Equivalent static wind loads; Non-Gaussian unsteady pressure field; Polynomial chaos expansion; Quasi-static responses; Stochastic dynamics; Extreme value statistics.

Notations

$\underline{\mathbf{f}}$	External force mean value
$\mathbb{f}^{e,s}$	Total equivalent static force
$\mathbf{f}^{e,s}$	Centered equivalent static force
$\underline{\mathbf{p}}$	Vector of the unsteady pressure mean value
$\underline{\mathbf{u}}$	Observation mean value
$\underline{\mathbf{y}}$	Displacement mean value
$[A_c]$	Controlability matrix
$[A_o]$	Observability matrix
$\mathbf{F}$	External forces vector
$\mathbb{F}^e$	Total equivalent force
$\mathbf{F}^e$	Centered equivalent force
$\mathbf{H}$	Coordinates of the PCA of $\mathbf{P}(T)$

*Corresponding author, Professor, E-mail: christian.soize@univ-paris-est.fr
[a]Ph.D., E-mail: wafaa.kassir@cstb.fr
[b]Doctor, E-mail: jean-vivien.heck@cstb.fr
[c]Doctor, E-mail: fabrice.de-oliveira@cstb.fr

$\mathbb{P}$	Total pressure vector-valued stochastic process
$\mathbf{P}$	Centered pressure vector-valued stochastic process
$\mathbb{P}^{\exp}$	Total experimental pressure vector-valued stochastic process
$\mathbf{P}^{\exp}$	Centered experimental pressure field
$\mathbf{Q}$	Centered generalized coordinates associated with $\mathbf{P}$
T	Time window duration in s
$\mathbb{U}$	Observation vector associated with $\mathbb{P}$
$\mathbf{U}$	Centered observation vector associated with $\mathbf{P}$
$\mathbf{X}$	Centered displacement vector associated with $\mathbf{P}$
$\mathbf{Y}$	Displacement vector associated with $\mathbb{P}$
Γ	Coordinates of the KL expansion of $\mathbf{P}$

1. Introduction

This paper deals with a novel approach for estimating the equivalent static wind loads (ESWL) on structures with complex aerodynamic flows such as stadium roofs, for which the pressure fields are measured in wind tunnels and are non-Gaussian, and for which the structural dynamic responses cannot simply be described by using only the first elastic modes (but require to introduce a good representation of the quasi-static responses).

Concerning the random responses of structures submitted to wind loads, once the first stochastic models of wind were developed, they were used to calculate the linear stochastic dynamical responses of tall buildings, introducing reduced modal models of the structure, and computing estimates of extreme value statistics related to the random dynamical responses. These estimates are based on using sample paths statistics of Gaussian processes that have allowed the "gust loading factor" concept to be introduced. Davenport (Davenport 1961) was the pioneer. Numerous studies have then been made by using the same assumptions but by improving models and conducting many experimental validations in full scale and in turbulent-boundary-layer wind tunnels, such as (Davenport 1961, 1967, Vickery and Danveport 1967, Vaicaitis *et al.* 1973, Solari 1985, Krée and Soize 1986, Kasperski and Niemann 1988, Holmes 1992, Kareem 1992, Davenport 1995, Bienkiewicz *et al.* 1995, Bietry *et al.* 1995, Solliec and Mary 1995, Simiu and Scanlan 1996, Uematsu *et al.* 1997, Ellingwood and Tekie 1999, Tamura *et al.* 1999) and more recently, (Kumar and Stathopoulos 2000, Vinet and De Oliveira 2011, Flamand *et al.* 2014, Vinet *et al.* 2015). Relatively early, several works were carried out to take into account the non-Gaussianity of the forces induced by the wind for the calculation of the extreme value statistics in stochastic dynamics by using formulations based on the use of gust loading factors (see for instance (Vaicaitis and Simiu 1977, Soize 1978, Krée and Soize 1986, Simiu and Scanlan 1996)). More recently, a lot of works have been performed for exceptional structures such as, for instance, the wind effects on super-tall buildings (Irwin 2009, Yi *et al.* 2013, Lu *et al.* 2016, Zhi *et al.* 2016), on super long-span cable bridges (Zhang and Yao *et al.* 2015), and on silo groups (Hillewaere *et al.* 2013, 2015).

Concerning the equivalent static wind loads, relatively early, late 60's and early 70's, research has been performed to develop methods for calculating the ESWL producing the same extreme dynamical responses of structures subjected to wind effects. The first proposed approaches were then

widely developed with many applications in civil engineering structures, such as (Simiu 2015, Cook and Mayne 1979, Kasperski and Niemann 1992, Kasperski 1992, Zhou *et al.* 1999a, b, Holmes 2002, Chen and Kareem 2004, Repetto and Solari 2004) and more recently, (Chen and Zhou 2007, Huang and Chen 2007, Katsumara *et al.* 2007, Uematsu *et al.* 2008, Fu *et al.* 2010, Zhou and Gu 2010, Blaise and Denoël 2013, Yang *et al.* 2013, Liang *et al.* 2014, Gu and Huang 2015, Sun *et al.* 2015, Patruno *et al.* 2017). In order to improve the estimation of the ESWL, some correction terms have been proposed to take into account the non-Gaussianity of the unsteady pressure field in order to calculate the extreme value statistics (Blaise and Denoël 2015, Lou *et al.* 2015, Blaise *et al.* 2016) using an orthogonal polynomial expansion of probability density functions (method that was already used in the 70's).

This paper deals with the design of structures subjected to wind effects for which the unsteady aerodynamic flow is complex, such as the one on a stadium roof. For such a case, it is still difficult to predict the aerodynamic flow with a sufficient accuracy by using computational fluid dynamics. This is the reason why measurements of the unsteady pressures on such structures are often necessary and must be carried out in wind tunnels. Most often, the number of unsteady pressure sensors, which are used for performing experimental measurements, is relatively high (about $1{,}000$). The number of the time trajectories (realizations) that are measured by the set of the pressure sensors and that are performed on long duration T (about 10 minutes in scale 1), remains limited (for instance between 25 and 100). Under these experimental conditions, the measurements do not allow for constructing a statistically converged estimation of the extreme values statistics of the dynamical responses, which are necessary for the estimation of the ESWL in order to reproduce the wind action on the structure taking into account the non-Gaussianity of the random pressure field. To circumvent such a difficulty, a general stochastic representation model of the non-Gaussian pressure field is constructed and is experimentally identified with the measurements. This stochastic representation model is then used for generating a large number of independent realizations (Monte-Carlo simulation method) in order to obtain a reasonable convergence of the extreme values statistics of the responses.

In this paper, a novel probabilistic approach is proposed to estimate the ESWL. Firstly, a generator of realizations of the non-Gaussian pressure random field is constructed by using the experiments. This generator allows to generate additional realizations to those measured in the wind tunnel. Secondly, the reduced-order dynamical model (ROM) of the structure includes a quasi-static correction term that allows the convergence of the stochastic dynamical responses to be obtained by using only a small number of elastic modes. Finally, the ESWL are estimated by a maximum probability principle related to the random displacements of the structure, conditioned by the random observations that have to belong to a domain representing the extreme values of the observations (internal forces, displacement, etc.) in the structure. The proposed method is validated on a simple example. At the end of this paper, an application to a roof stadium structure, for which pressure measurements in wind tunnel are available, is presented in order to illustrate the proposed method.

2. Stochastic modeling, model reduction, and stationary stochastic response

In this section, we first present the stochastic modeling of the pressure and then, we introduce the ROM in the time domain that will be used for constructing the realizations of the time responses. For such a calculation, two algorithms can be used: time integration scheme applied to the time differential equation or the fast Fourier transform (FFT) for each realization, which can be used because we are interested in the stationary response of the stochastic dynamical system. The second algorithm is more numerically efficient and will be retained.

In this paper, for the stochastic modeling, any stochastic process $\{\mathbf{V}(t), t \in \mathbb{R}\}$ (simply called process) is defined on a probability space $(\Theta, \mathscr{T}, \mathscr{P})$ [1] and is stationary. Its restriction to the time window $[0\,, T]$ of duration T (defined hereinafter) will be denoted by $\{\mathbf{V}(t), t \in [0\,, T]\}$. A realization θ_ℓ in Θ of process $\{\mathbf{V}(t), t \in [0\,, T]\}$ is the deterministic function $\{\mathbf{V}(t; \theta_\ell), t \in [0\,, T]\}$. Similarly, for the centered experimental measurements, process $\{\mathbf{P}^{\exp}(t), t \in [0\,, T]\}$ is defined on another probability space $(\Theta', \mathscr{T}', \mathscr{P}')$, for which any realization θ'_ℓ in Θ' is the deterministic function $\{\mathbf{P}^{\exp}(t; \theta'_\ell), t \in [0,\, T]\}$.

Let $\mathbf{F}(t) = (F_1(t), \ldots, F_m(t))$ be the vector of external wind forces (forces and/or bending moments) applied to the structure, which is written as $\mathbf{F}(t) = [A_c]\, \mathbb{P}^{\exp}(t)$ in which $[A_c]$ is the $(m \times m_{\exp})$ controllability matrix and where $\mathbb{P}^{\exp}(t) = (\mathbb{P}_1^{\exp}(t), \ldots, \mathbb{P}_{m_{\exp}}^{\exp}(t))$ is the vector that corresponds to the wind tunnel unsteady pressure measurements or to differential unsteady pressures at some points of the structure (Vinet and De Oliveira 2011, Vinet *et al.* 2015).

Concerning the signal processing parameters, the total duration of the time acquisition of measurements is T_{tot} and the experimental unsteady pressure vector is a deterministic function denoted by $t \mapsto \mathfrak{p}^{\exp}(t)$ from $[0, T_{\text{tot}}]$ into $\mathbb{R}^{m_{\exp}}$. The cutoff frequency is ν_c with $\omega_c = 2\pi\nu_c$ in which the frequency band of analysis is $\mathscr{B} = [0, \omega_c]$ (in rad/s). The sampling time step is $\Delta t = 1/2\nu_c$ and the number of time steps for the time sampling of $[0\,, T]$ is n_p such that $T = n_p\, \Delta t$. The time sampling points are $t_1, \ldots, t_{n_p}$ with $t_1 = 0$ and $t_k = (k-1)\, \Delta$ of $[0, T]$ for $k = 2, \ldots, n_p$. The frequency sampling points are $\omega_q = -\omega_c + (q - \frac{1}{2})\Delta\omega$ with $q = 1, \ldots, n_p$ in which $\Delta\omega = 2\pi/T$. These parameters allow for defining n_r time-sampled realizations $\mathbb{P}^{\exp}(t_k; \theta'_\ell)$ with $k = 1, \ldots, n_p$ and $\ell = 1, \ldots, n_r$ of process $\{\mathbb{P}^{\exp}(t), t \in [0, T]\}$ such that $\mathbb{P}^{\exp}(t_k; \theta'_\ell) = \mathfrak{p}^{\exp}(t_k + (\ell - 1)\, T)$ in which the number of realizations is defined by $T_{\text{tot}} = n_r \times T$.

The vector-valued process $\mathbb{P}^{\exp}$ of the pressure measurements is modeled by a stationary non-Gaussian process $\mathbb{P} = \{\mathbb{P}(t), t \in \mathbb{R}\}$ with $\mathbb{P}(t) = (\mathbb{P}_1(t), \ldots, \mathbb{P}_{m_{\exp}}(t))$. The non-Gaussian centered process $\mathbf{P} = \{\mathbf{P}(t), t \in \mathbb{R}\}$ such that $\mathbf{P}(t) = (P_1(t), \ldots, P_{m_{\exp}}(t))$ is then defined by

$$\mathbb{P}(t) = \underline{\mathbf{p}} + \mathbf{P}(t) \quad , \quad \underline{\mathbf{p}} \simeq \frac{1}{n_r} \sum_{\ell=1}^{n_r} \frac{1}{n_p} \sum_{k=1}^{n_p} \mathbb{P}^{\exp}(t_k; \theta'_\ell)\,, \tag{1}$$

where $\underline{\mathbf{p}}$ is the static part of $\mathbb{P}$. The structure is fixed (no rigid body displacement) and its computational linear dynamical model has m degrees of freedom (DOF). Let $\mathbf{Y}(t) = (Y_1(t), \ldots, Y_m(t))$ be

[1] In the probability space $(\Theta, \mathscr{T}, \mathscr{P})$, Θ is set of all the elementary events, $\mathscr{T}$ is the σ-algebra of Θ whose elements are called events, and $\mathscr{P}$ is a probability measure on measurable space $(\Theta, \mathscr{T})$. For t fixed, the $\mathbb{R}^n$-valued random variable $\mathbf{V}(t)$ is a measurable mapping $\theta \mapsto \mathbf{V}(t; \theta)$ from $(\Theta, \mathscr{T})$ into $(\mathbb{R}^n, \mathscr{B}_n)$ in which $\mathscr{B}_n$ is the Borel σ-algebra of $\mathbb{R}^n$. For θ fixed in Θ, $\mathbf{V}(t; \theta)$ is a realization of random vector $\mathbf{V}(t)$ and $\{\mathbf{V}(t; \theta), t \in [0\,, T]\}$ is a trajectory (or a sample path) of stochastic process $\mathbf{V}$.

the displacement vector (translations and/or rotations). The components of an observation $\mathbb{U}(t) = (\mathbb{U}_1(t), \ldots, \mathbb{U}_{m_u}(t))$ in the structure can be displacements, internal forces, stresses or strains and is written as $\mathbb{U}(t) = [A_o]\,\mathbf{Y}(t)$ in which $[A_o]$ is the $(m_u \times m)$ observability matrix. The non usual modal analysis including a quasi-static term (Ohayon and Soize 1998) is used for constructing the ROM with N first elastic modes whose eigenfrequencies lye in $\mathscr{B}$. The response $\mathbf{Y}(t)$ is written as $\mathbf{Y}(t) = \underline{\mathbf{y}} + \mathbf{X}(t)$, where the static response $\underline{\mathbf{y}}$ is such that $[K]\,\underline{\mathbf{y}} = \underline{\mathbf{f}}$ with $\underline{\mathbf{f}} = [A_c]\,\underline{\mathbf{p}}$, and where $[K]$ is the $(m \times m)$ stiffness matrix. The displacement vector $\mathbf{X}(t) = (X_1(t), \ldots, X_m(t))$ is the non-Gaussian stationary centered process that, for all t, verifies

$$\mathbf{X}(t) = [\mathscr{S}_N^c]\,\mathbf{P}(t) + [\varphi_N]\,\mathbf{Q}(t)\,, \tag{2}$$

$$\ddot{\mathbf{Q}}(t) + [D_N]\,\dot{\mathbf{Q}}(t) + [\lambda_N]\,\mathbf{Q}(t) = \boldsymbol{\mathscr{P}}_N^c(t)\,, \tag{3}$$

in which $\mathbf{Q}(t) = (Q_1(t), \ldots, Q_N(t))$ is a non-Gaussian stationary centered process of the generalized coordinates, where $[\varphi_N]$ is the $(m \times N)$ matrix of the elastic modes normalized with respect to the mass matrix, where $[\lambda_N]$ is the $(N \times N)$ diagonal matrix of the square of the eigenfrequencies $\Omega_1, \ldots, \Omega_N$, where $[D_N]_{\alpha\beta} = 2\xi_\alpha\Omega_\alpha\delta_{\alpha\beta}$ is the $(N \times N)$ diagonal matrix of the generalized damping depending on the damping rates $\xi_1, \ldots, \xi_N$, where $\boldsymbol{\mathscr{P}}_N^c(t) = [\phi_N^c]\,\mathbf{P}(t)$ with $[\phi_N^c] = [\varphi_N]^T\,[A_c]$, and where the $(m \times m_{\text{exp}})$ matrix $[\mathscr{S}_N^c] = [K]^{-1}\,[A_c] - [\varphi_N]\,[\lambda_N]^{-1}\,[\phi_N^c]$ represents the quasi-static terms (note that the sparse stiffness matrix $[K]$ will never be inverted). Observation $\mathbb{U}(t)$ is written as

$$\mathbb{U}(t) = \underline{\mathbf{u}} + \mathbf{U}(t) \quad , \quad \mathbf{U}(t) = [\mathscr{U}_N^{oc}]\,\mathbf{P}(t) + [\phi_N^o]\,\mathbf{Q}(t)\,, \tag{4}$$

in which $[\mathscr{U}_N^{oc}] = [A_o][\mathscr{S}_N^c]$, $[\phi_N^o] = [A_o]\,[\varphi_N]$, and where $\underline{\mathbf{u}} = (\underline{u}_1, \ldots, \underline{u}_{m_u})$ is the static part of $\mathbb{U}$ such that $\underline{\mathbf{u}} = [A_o]\,\underline{\mathbf{y}}$. At time t, the instantaneous ESWL that is denoted by $\mathbb{F}^e(t) = (\mathbb{F}_1^e(t), \ldots, \mathbb{F}_m^e(t))$ and defined by $\mathbb{F}^e(t) = [K]\,\mathbf{Y}(t)$, is written as

$$\mathbb{F}^e(t) = \underline{\mathbf{f}} + \mathbf{F}^e(t) \quad , \quad \mathbf{F}^e(t) = [K]\,\mathbf{X}(t)\,, \tag{5}$$

where $\underline{\mathbf{f}}$ is the static part of $\mathbb{F}^e$ given by $[K]\,\underline{\mathbf{y}} = \underline{\mathbf{f}}$. From Eqs. (2), (3), and (5), it can be deduced that

$$\mathbf{F}^e(t) = [\mathscr{F}_N^c]\,\mathbf{P}(t) + [\mathcal{F}_N^{\mathbf{Q}}]\mathbf{Q}(t)\,, \tag{6}$$

in which $[\mathcal{F}_N^{\mathbf{Q}}] = [K]\,[\varphi_N]$ and where $[\mathscr{F}_N^c] = [K]\,[\mathscr{S}_N^c]$. For given θ_ℓ in Θ, the realization $\{\mathbf{Q}(t;\theta_\ell), t \in [0\,,T]\}$ is computed at the time sampling points $t_1, \ldots, t_{n_p}$ by using its discrete FFT $\widehat{\mathbf{Q}}(\omega_q;\theta_\ell) = [\widehat{h}_N(\omega_q)]\widehat{\boldsymbol{\mathscr{P}}}_N^c(\omega_q;\theta_\ell)$ with $q = 1, \ldots, n_p$, where $\widehat{\boldsymbol{\mathscr{P}}}_N^c(\omega_q;\theta_\ell)$ is computed by using the FFT at the time sampling points $t_1, \ldots, t_{n_p}$ of $\{\boldsymbol{\mathscr{P}}_N^c(t;\theta_\ell), t \in [0,T]\}$, and where $[\widehat{h}_N(\omega)]_{\alpha\beta} = \delta_{\alpha\beta}(-\omega^2 + 2i\omega\xi_\alpha\Omega_\alpha + \Omega_\alpha^2)^{-1}$ with $\delta_{\alpha\beta}$ the Kronecker symbol. For $k = 1, \ldots, n_p$, the discretized realization $\mathbf{Q}(t_k;\theta_\ell)$ of $\{\mathbf{Q}(t;\theta_\ell), t \in [0\,,T]\}$ is deduced by the inverse FFT.

3. Generator of additional realizations of non-Gaussian process P

As explained in Section 1, the n_r experimental time sampled realizations $\{\mathbb{P}^{\text{exp}}(t_k;\theta'_\ell), \ell = 1, \ldots, n_r\}$ are generally not sufficient for estimating the extreme values statistics of the responses, which are required for computing the ESWL. It is then necessary to generate $\nu \gg n_r$ time sampled

realizations $\{\mathbf{P}(t_k;\theta_\ell), \ell = 1,\ldots,\nu\}$ of the centered process $\mathbf{P}$ with a non-Gaussian generator. Using the n_r experiments $\mathbb{P}^{\exp}(t_k;\theta'_\ell)$, the methodology consists in performing a Karhunen-Loève (KL) statistical reduction of non-Gaussian process $\mathbf{P}$ and then in identifying a representation of the random vector of the KL coordinates by a finite polynomial chaos expansion (PCE) (Ghanem and Spanos 1991). The coefficients of the PCE are estimated with the maximum likelihood principle (Desceliers *et al.* 2006, Perrin *et al.* 2012, Soize 2017). The maximum likelihood optimization problem can be solved either by using a random search algorithm or by using a deterministic optimization such as the "interior points" method (Byrd *et al.* 1999). The KL statistical reduction of order N_{KL} of $\{\mathbf{P}(t), t \in [0,T]\}$ is written as,

$$\mathbf{P}(t) \simeq \sum_{j=1}^{N_{\mathrm{KL}}} \sqrt{\mu_j}\,\Gamma_j \mathbf{b}^j(t) \quad , \quad t \in [0,T]\,, \tag{7}$$

in which $\{\mu_j, \mathbf{b}^j\}$ are the solutions of the functional eigenvalue problem

$$\frac{1}{T}\int_0^T [C_{\mathbf{P}}(t-t')]\,\mathbf{b}^j(t')\,dt' = \mu_j\,\mathbf{b}^j(t) \quad , \quad \forall t \in [0,T]\,, \tag{8}$$

with $[C_{\mathbf{P}}(t-t')] = E\{\mathbf{P}(t)\,\mathbf{P}(t')^T\}$ in which E is the mathematical expectation, and where the corrdinates $\mathbf{\Gamma} = (\Gamma_1,\ldots,\Gamma_{N_{\mathrm{KL}}})$ of this KL reduction is a non-Gaussian random vector with values in $\mathbb{R}^{N_{\mathrm{KL}}}$ such that $E\{\mathbf{\Gamma}\} = \mathbf{0}$ and $E\{\mathbf{\Gamma}\,\mathbf{\Gamma}^T\} = [I_{N_{\mathrm{KL}}}]$ with $[I_{N_{\mathrm{KL}}}]$ the identity matrix. The eigenvalue problem defined by Eq. (8) is indirectly solved by using an algorithm (Andrews and Patterson 1976) based on the thin SVD (Golub and Van Loan 2013), which is directly applied to the time sampled realizations $\mathbf{P}^{\exp}(t_k;\theta'_\ell) = \mathbb{P}^{\exp}(t_k;\theta'_\ell) - \underline{\mathbf{p}}$ (see (Kassir 2017)). Let $\mathbf{\Xi} = (\Xi_1,\ldots,\Xi_{N_g})$ be the normalized Gaussian random germ of length N_g defined on $(\Theta, \mathscr{T}, \mathscr{P})$, used for constructing the PCE of $\mathbf{\Gamma}$. Let $\Psi_{\boldsymbol{\beta}}(\mathbf{\Xi}) = \psi_{\beta_1}(\Xi_1)\times\ldots\times\psi_{\beta_{N_g}}(\Xi_{N_g})$ be the Hermite orthonormal polynomials where $\boldsymbol{\beta} = (\beta_1,\ldots,\beta_{N_g})$ is the multi-index of length N_g such that, for $j = 1,\ldots,N_g$, $\beta_j \in \{0,1,\ldots,N_d\}$ with $N_d \geq 1$ a fixed integer corresponding to the maximum degree of the polynomials. This choice is dictated by the fact that the Gaussian approximation can directly be obtained by taking only the polynomials of degree zero and one, which would not be the case if non-Gaussian germ were taken. The approximation of $\mathbf{\Gamma}$, using the PCE, is written as

$$\mathbf{\Gamma} \simeq \sum_{\kappa=1}^{K(N_d,N_g)} \mathbf{z}^{\kappa}\,\Psi_{\boldsymbol{\beta}^{(\kappa)}}(\mathbf{\Xi})\,, \tag{9}$$

in which $K(N_d,N_g) = (N_g+N_d)!/N_g!\,N_d! - 1$ and where, as previously explained, the coefficients $\mathbf{z}^1,\ldots,\mathbf{z}^{K(N_d,N_g)}$ are deterministic vectors in $\mathbb{R}^{N_{\mathrm{KL}}}$ estimated from the experimental measurements using the maximum likelihood principle (Kassir 2017). We then have constructed the non-Gaussian generator that is used as follows. Let $\mathbf{\Xi}(\theta_1),\ldots,\mathbf{\Xi}(\theta_\nu)$ be ν independent realizations of $\mathbf{\Xi}$. For $k = 1,\ldots,n_p$, the ν independent realizations of non-Gaussian random vectors $\{\mathbf{P}(t_k), k = 1,\ldots,n_p\}$ are computed by

$$\mathbf{P}(t_k;\theta_\ell) \simeq \sum_{j=1}^{N_{\mathrm{KL}}} \sqrt{\mu_j}\,\Gamma_j(\theta_\ell)\,\mathbf{b}^j(t_k) \quad , \quad \ell = 1,\ldots,\nu\,, \tag{10}$$

in which $\mathbf{\Gamma}(\theta_\ell) = (\Gamma_1(\theta_\ell), \ldots, \Gamma_{N_{\rm KL}}(\theta_\ell))$ is the ℓ-th realization of $\mathbf{\Gamma}$ that is computed by

$$\mathbf{\Gamma}(\theta_\ell) \simeq \sum_{\kappa=1}^{K(N_d,N_g)} \mathbf{z}^\kappa \, \Psi_{\boldsymbol{\beta}^{(\kappa)}}(\boldsymbol{\Xi}(\theta_\ell)) \, . \tag{11}$$

4. Estimation of the equivalent static wind loads

Taking into account Eq. (5), the equivalent static wind load $\mathbb{f}^{e,s} = (\mathbb{f}_1^{e,s}, \ldots, \mathbb{f}_m^{e,s})$ associated with observation $\mathbb{U}$, is written as $\mathbb{f}^{e,s} = \underline{\mathbb{f}} + \mathbf{f}^{e,s}$. The instantaneous centered ESWL at time $t = T$ is written as $\mathbf{F}^e(T) = [\mathscr{F}_N^c]\,\mathbf{P}(T) + [\mathcal{F}_N^{\mathbf{Q}}]\mathbf{Q}(T)$. As the dimension $m_{\rm exp}$ of the random vector $\mathbf{P}(T)$ is much larger (for instance 700 to 1,000) than the dimension of $\mathbf{Q}(T)$ and $\mathbf{U}(T)$, a principal component analysis (PCA) of random vector $\mathbf{P}(T)$ is introduced in order to reduce the statistical dimension and to normalize the random quantities,

$$\mathbf{P}(T) \simeq \underline{\mathbf{p}}_T + \sum_{j=1}^{N_{\rm PCA}} \sqrt{\Lambda_j}\, H_j\, \mathbf{a}^j \, , \tag{12}$$

in which $N_{\rm PCA}$ is the reduction order such that $N_{\rm PCA} \leq m_{\rm exp}$, $\underline{\mathbf{p}}_T$ is the empirical mean of $\mathbf{P}(T)$, $(\mathbf{a}^1, \ldots, \mathbf{a}^{N_{\rm PCA}})$ are the eigenvectors associated with the $N_{\rm PCA}$ largest eigenvalues $\Lambda_1 \geq \Lambda_2 \geq \ldots \geq \Lambda_{N_{\rm PCA}}$ of the estimate of the covariance matrix $[C_{\mathbf{P}(T)}]$ of $\mathbf{P}(T)$, and $\mathbf{H} = (H_1, \ldots, H_{N_{\rm PCA}})$ is the random coordinates of the PCA. As explained in Section 1, the equivalent static wind load $\mathbf{f}^{e,s}$ is estimated by using the following maximum probability principle,

$$\mathbf{f}^{e,s} = [\mathscr{F}_N^c]\,\mathbf{p}^{\rm MV} + [\mathcal{F}_N^{\mathbf{Q}}]\,\mathbf{q}^{\rm MV} \quad \text{with} \quad \mathbf{p}^{\rm MV} \simeq \underline{\mathbf{p}}_T + \sum_{j=1}^{N_{\rm PCA}} \sqrt{\Lambda_j}\,\eta_j^{\rm MV}\,\mathbf{a}^j \, , \tag{13}$$

in which the vectors $\boldsymbol{\eta}^{\rm MV} = (\eta_1^{\rm MV}, \ldots, \eta_{N_{\rm PCA}}^{\rm MV})$ and $\mathbf{q}^{\rm MV} = (q_1^{\rm MV}, \ldots, q_N^{\rm MV})$ are such that

$$(\boldsymbol{\eta}^{\rm MV}, \mathbf{q}^{\rm MV}) = \arg\{\max_{(\boldsymbol{\eta},\mathbf{q})} \int_{\mathscr{D}^c} p_{\mathbf{H},\mathbf{Q}(T),\mathbf{U}(T)}(\boldsymbol{\eta}, \mathbf{q}, \mathbf{u})\, d\mathbf{u}\} \, , \tag{14}$$

where $p_{\mathbf{H},\mathbf{Q}(T),\mathbf{U}(T)}(\boldsymbol{\eta}, \mathbf{q}, \mathbf{u})$ is the joint probability density function of random vectors $\mathbf{H}$, $\mathbf{Q}(T)$, $\mathbf{U}(T)$, and where $\mathscr{D}^c$ is the centered domain associated with $\mathbf{U}$, which is assumed to be written as a Cartesian product: $\mathscr{D}^c = \Pi_{j=1}^{m_u} \mathscr{D}_j^c$ with $\mathscr{D}_j^c = (\mathscr{D}_{{\rm inf},j}^c, \mathscr{D}_{{\rm sup},j}^c)$ where $\mathscr{D}_{{\rm inf},j}^c$ and $\mathscr{D}_{{\rm sup},j}^c$ are the lower and the upper bounds of $\mathscr{D}_j^c$. For $j = 1, \ldots, m_u$, the bounds $\mathscr{D}_{{\rm inf},j}^c$ and $\mathscr{D}_{{\rm sup},j}^c$ are defined with respect to the sign of the mean observation $\underline{u}_j$ as follows

$$\begin{array}{lllll} \text{if} \quad \underline{u}_j \geq 0 \quad , & \text{then} & \mathscr{D}_{{\rm inf},j}^c = \underline{U}_{{\rm max},j} \quad , & \mathscr{D}_{{\rm sup},j}^c = \alpha \underline{U}_{{\rm max},j} \, , \\ \text{if} \quad \underline{u}_j < 0 \quad , & \text{then} & \mathscr{D}_{{\rm inf},j}^c = \alpha \underline{U}_{{\rm min},j} \quad , & \mathscr{D}_{{\rm sup},j}^c = \underline{U}_{{\rm min},j} \, , \end{array} \tag{15}$$

where $\underline{U}_{{\rm max},j}$ (resp. $\underline{U}_{{\rm min},j}$) is the mean value of the maximum (resp. the minimum) of $U_j(t)$ on $[0, T]$, and where α is a positive constant (for instance $\alpha = 1{,}000$). In order to accelerate the

convergence of the optimizer used for solving the problem defined by Eq. (14), we superimpose a constraint on vector $\mathbf{U}(T)$ by introducing the following admissible set for the values of $(\mathbf{H}, \mathbf{Q}(T))$,

$$\mathscr{C}_{\boldsymbol{\eta}\mathbf{q}} = \{(\boldsymbol{\eta}, \mathbf{q}) \in \mathbb{R}^{N_{\text{PCA}}} \times \mathbb{R}^N ; \mathbf{u} \in \mathscr{D}^c\} \,. \tag{16}$$

Therefore, in Eq. (14), the maximization on $(\boldsymbol{\eta}, \mathbf{q}) \in \mathbb{R}^{N_{\text{PCA}}} \times \mathbb{R}^N$ is replaced by the maximization on $(\boldsymbol{\eta}, \mathbf{q}) \in \mathscr{C}_{\boldsymbol{\eta}\mathbf{q}}$ and the non-Gaussian joint probability density function is estimated using the Gaussian kernel method of the non-parametric statistics (Givens and Hoeting 2013) and the integration over set $\mathscr{D}^c$ is explicitly (algebraically) calculated (Kassir 2017). The optimization problem is solved using the "active set" algorithm without constraints (Gill *et al.* 1981). The ESWL are estimated for $m_{\mathbb{f}}$ observations $\{\mathbb{U}^i(T), \mathscr{D}_i\}$ with $i = 1, \ldots, m_{\mathbb{f}}$ and the associated principal static wind loads are classically computed by SVD.

5. Construction of the initial point of the optimization problem

The numerical cost requires for solving Eq. (14) can considerably be reduced if the initial point is well chosen for the optimizer. Below, we propose a very efficient algorithm for computing the initial point. Let $\mathbf{Z}$ be the $\mathbb{R}^n$-valued random variable defined by $\mathbf{Z} = (\mathbf{H}, \mathbf{Q}(T), \mathbf{U}(T))$ with $n = N_{\text{PCA}} + N + m_u$. The estimate of the covariance matrix $[C_{\mathbf{Z}}]$ of $\mathbf{Z}$ is written as $[C_{\mathbf{Z}}] = [\sigma]\,[r_{\mathbf{Z}}]\,[\sigma]$ in which $[\sigma]_{jk} = \delta_{jk}\,\sigma_j$ with $\sigma_j = [C_{\mathbf{Z}}]_{jj}^{1/2}$, and where $[r_{\mathbf{Z}}]$ is the estimate of the correlation matrix of $\mathbf{Z}$ such that $[r_{\mathbf{Z}}]_{jk} = [C_{\mathbf{Z}}]_{jk}/(\sigma_j \sigma_k)$. Let $\{\mathbf{z}^\ell = (\boldsymbol{\eta}^\ell, \mathbf{q}^\ell, \mathbf{u}^\ell), \ell = 1, \ldots, \nu\}$ be the ν independent realizations of $\mathbf{Z}$. We need to introduce the PCA of the $\mathbb{R}^n$-valued random variable $\mathbf{Z}$ based on the estimate of $[C_{\mathbf{Z}}]$. Since, the numerical values of the realizations of $\mathbf{H}$ and $\mathbf{Q}(T)$ can be very different (several magnitude orders), a numerical scaling defined by $[\sigma]$ is introduced and the PCA of $\mathbf{Z}$ is then written as

$$\mathbf{Z} = \underline{\mathbf{z}} + \sum_{\alpha=1}^{n} \zeta_\alpha \sqrt{a_\alpha}\, \boldsymbol{\Psi}^\alpha \,, \tag{17}$$

in which $\underline{\mathbf{z}}$ is the mean value of $\mathbf{Z}$, a_α and $\boldsymbol{\Psi}^\alpha$ are the eigenvalue and the eigenvector of $[C_{\mathbf{Z}}]$ such that $([\sigma]^{-2}\boldsymbol{\Psi}^\alpha)^T \boldsymbol{\Psi}^\beta = \delta_{\alpha\beta}$, and where $\zeta_1, \ldots, \zeta_n$ are the uncorrelated centered random variables with unit variances, which are such that $\zeta_\alpha = a_\alpha^{-1/2} < [\sigma]^{-2}(\mathbf{Z} - \underline{\mathbf{z}}), \boldsymbol{\Psi}^\alpha >$. Let $\mathbf{Z}^{(m_u)}$ be the approximation defined by

$$\mathbf{Z}^{(m_u)} = \underline{\mathbf{z}} + \sum_{\alpha=1}^{m_u} \zeta_\alpha \sqrt{a_\alpha}\, \boldsymbol{\Psi}^\alpha \,. \tag{18}$$

By introducing the decomposition $\mathbf{Z}^{(m_u)} = (\mathbf{H}^{(m_u)}, \mathbf{Q}^{(m_u)}(T), \mathbf{U}^{(m_u)}(T))$, the $\mathbb{R}^{N_{\text{PCA}}}$-valued random variable $\mathbf{H}^{(m_u)}$ and the $\mathbb{R}^N$-valued random variable $\mathbf{Q}^{(m_u)}(T)$ can be written as,

$$\mathbf{H}^{(m_u)} = \mathbf{m}_{\mathbf{H}} + \sum_{\alpha=1}^{m_u} \zeta_\alpha \sqrt{a_\alpha}\, \boldsymbol{\Psi}^\alpha_{\mathbf{H}} \quad , \quad \mathbf{Q}^{(m_u)}(T) = \mathbf{m}_{\mathbf{Q}(T)} + \sum_{\alpha=1}^{m_u} \zeta_\alpha \sqrt{a_\alpha}\, \boldsymbol{\Psi}^\alpha_{\mathbf{Q}(T)} \,, \tag{19}$$

and the $\mathbb{R}^{m_u}$-valued random variable $\mathbf{U}^{(m_u)}(T)$ can be written as,

$$\mathbf{U}^{(m_u)}(T) = \mathbf{m}_{\mathbf{U}(T)} + \sum_{\alpha=1}^{m_u} \zeta_\alpha \sqrt{a_\alpha}\, \boldsymbol{\Psi}^\alpha_{\mathbf{U}(T)} \,, \tag{20}$$

where $\underline{\mathbf{z}} = (\mathbf{m}_{\mathbf{H}}, \mathbf{m}_{\mathbf{Q}(T)}, \mathbf{m}_{\mathbf{U}(T)})$ and $\boldsymbol{\Psi}^\alpha = (\boldsymbol{\Psi}^\alpha_{\mathbf{H}}, \boldsymbol{\Psi}^\alpha_{\mathbf{Q}(T)}, \boldsymbol{\Psi}^\alpha_{\mathbf{U}(T)})$. Let $[\Phi_{\mathbf{H}}]$, $[\Phi_{\mathbf{Q}(T)}]$, and $[\Phi_{\mathbf{U}(T)}]$ be the matrices such that

$$[\Phi_{\mathbf{H}}] = [\boldsymbol{\Psi}^1_{\mathbf{H}} \dots \boldsymbol{\Psi}^{m_u}_{\mathbf{H}}] \ , \ [\Phi_{\mathbf{Q}(T)}] = [\boldsymbol{\Psi}^1_{\mathbf{Q}(T)} \dots \Psi^{m_u}_{\mathbf{Q}(T)}] \ , \ [\Phi_{\mathbf{U}(T)}] = [\boldsymbol{\Psi}^1_{\mathbf{U}(T)} \dots \Psi^{m_u}_{\mathbf{U}(T)}] \, . \tag{21}$$

In matrix form, Eq. (20) can then be rewritten as

$$\mathbf{U}^{(m_u)}(T) = \mathbf{m}_{\mathbf{U}(T)} + [\Phi_{\mathbf{U}(T)}] \, [\, a \,]^{1/2} \, \boldsymbol{\zeta} \, , \tag{22}$$

in which $[\, a \,]_{\alpha\beta} = a_\alpha \, \delta_{\alpha\beta}$ and where $\boldsymbol{\zeta} = (\zeta_1, \dots, \zeta_{m_u})$ is the centered $\mathbb{R}^{m_u}$-valued random variable such that $E\{\boldsymbol{\zeta} \, \boldsymbol{\zeta}^T\} = [I_{m_u}]$. Let $\mathbf{u}^0 = (u^0_1, \dots, u^0_{m_u})$ be such that $u^0_j = \underline{U}_{\max,j}$ if $\underline{u}_j \geq 0$ and $u^0_j = \underline{U}_{\min,j}$ if $\underline{u}_j < 0$. Taking into account Eq. (22), we introduce the deterministic vector $\mathbf{z}^0$ in $\mathbb{R}^{m_u}$ as the solution of the following optimization problem for minimizing the distance between $\mathbf{u}^0$and $\mathbf{U}^{(m_u)}(T)$,

$$\mathbf{z}^0 = \min_{\mathbf{z} \in \mathbb{R}^{m_u}} \| \mathbf{u}^0 - \mathbf{m}_{\mathbf{U}(T)} - [\Phi_{\mathbf{U}(T)}] \, [\, a \,]^{1/2} \, \mathbf{z} \|^2 \, . \tag{23}$$

Since $\{\boldsymbol{\Psi}^\alpha\}_\alpha$ is a basis of the space $\mathbb{R}^n$, this implies that $[\Phi_{\mathbf{U}(T)}]$ is an invertible matrix. Then the square matrix $[\Phi_{\mathbf{U}(T)}] \, [\, a \,]^{1/2}$ is invertible. The problem defined by Eq. (23) is then equivalent to solve the linear equation in $\mathbf{z}$, $[\Phi_{\mathbf{U}(T)}] \, [\, a \,]^{1/2} \, \mathbf{z} = \mathbf{u}^0 - \mathbf{m}_{\mathbf{U}(T)}$, which has a unique solution $\mathbf{z}^0$. We formally write $\mathbf{z}^0 = ([\Phi_{\mathbf{U}(T)}] \, [\, a \,]^{1/2})^{-1} \, (\mathbf{u}^0 - \mathbf{m}_{\mathbf{U}(T)})$, and Eq. (19) is rewritten as $\mathbf{H}^{(m_u)} = \mathbf{m}_{\mathbf{H}} + [\Phi_{\mathbf{H}}] \, [\, a \,]^{1/2} \, \boldsymbol{\zeta}$ and $\mathbf{Q}^{(m_u)}(T) = \mathbf{m}_{\mathbf{Q}(T)} + [\Phi_{\mathbf{Q}(T)}] \, [\, a \,]^{1/2} \, \boldsymbol{\zeta}$. The initial point $(\boldsymbol{\eta}^0, \mathbf{q}^0) \in \mathbb{R}^{N_{\text{PCA}}} \times \mathbb{R}^N$ of the optimization problem defined by Eq. (14) is then calculated by

$$\boldsymbol{\eta}^0 = \mathbf{m}_{\mathbf{H}} + [\Phi_{\mathbf{H}}] \, [\, a \,]^{1/2} \, \mathbf{z}^0 \quad , \quad \mathbf{q}^0 = \mathbf{m}_{\mathbf{Q}(T)} + [\Phi_{\mathbf{Q}(T)}] \, [\, a \,]^{1/2} \, \mathbf{z}^0 \, . \tag{24}$$

6. Experimental validation of the proposed methodology

A first step of the validation of the proposed theory and of the developed associated software have been carried out on a tall building, the Maine-Montparnasse Tower in Paris, for which experimental measurements have been performed by CEBTP (1978). The two first eigenfrequencies have been measured. For the measured value $\underline{V}_R = 17$ m/s of the reference mean wind velocity, the time responses have been measured for several sequences of 800 s concerning the relative horizontal displacement at the top of the Tower. The wind velocity model, the pressure modeling, and the updated computational reduced-order model presented in (Krée and Soize 1986) have been reused. The details of the modeling and of the experimental comparisons by using the proposed approach can be found in (Kassir *et al.* 2017, Kassir 2017). The extreme value statistics match very well the numerical predictions. This good experimental comparison participates to the validation of the proposed approach.

7. Application to a stadium roof structure with wind tunnel pressure measurements

The structure is the roof of the Allianz Riviera stadium in Nice for which unsteady pressure measurements have been performed in a boundary layer wind tunnel (Vinet and De Oliveira 2013) (see figure Fig. 1). The ROM presented in Section 2 has been constructed by using the finite element model provided by CSTB. The experimental cutoff frequency is 1.38 Hz and is chosen as a cutoff

Fig. 1 Model of the roof of the Allianz Riviera stadium in the boundary layer wind tunnel at CSTB in Nantes (Vinet and De Oliveira 2013).

frequency ν_c for the computational model. The eigenfrequencies of the first 12 modes, which lye in the frequency band of analysis $[0\,,1.38]$ Hz are taken into account in the ROM; we thus have $N = 12$. These eigenfrequencies, in Hz, are 1.107, 1.118, 1.129, 1.133, 1.148, 1.186, 1.191, 1.240, 1.248, 1.264, 1.349, and 1.360. The 13-th eigenfrequency is 1.416 Hz that is outside the frequency band of analysis. The quasi-static acceleration term is taken into account in the ROM.

7.1 Finite element model of the structure and set of observations

The FE model, given in an orthonormal reference frame $oxyz$, is made up of truss and beam elements. There are $3{,}656$ nodes with 6 degrees of freedom per node, which yields $21{,}936$ DOFs. Fig. 2 (left) shows the finite element model of the roof structure.The observed zone in the structure is shown in light color in Fig. 2 (left) and the detailed FE model of this zone is shown in Fig. 2 (right). The calculation of the ESWL is performed by using $m_{\mathbb{f}} = 181$ selected observations that are internal forces in truss and beam elements. In order to limit the number of figures, only four observations, numbered 144 to 147 (see Fig. 2 (right)) , which correspond to normal forces in truss elements, are presented. Consequently, each one is scalar (then $m_{u^i} = 1$) and is written as $\mathbb{U}^i(t) = \underline{u}^i + U^i(t)$ in which $\underline{u}^i$ is the mean value.

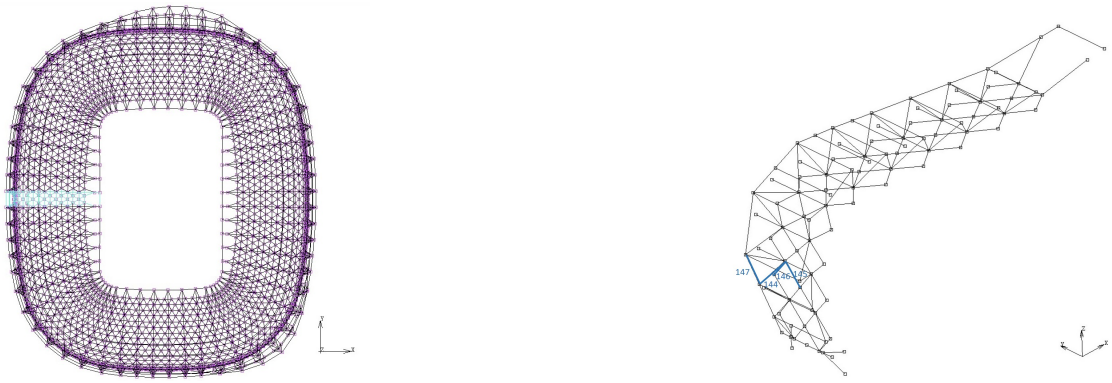

Fig. 2 Finite element model of the roof structure (left) and zoom (right) in the structural zone corresponding to the light color part shown in the left figure (from CSTB).

7.2 Wind tunnel measurements and values of the signal processing parameters

For incidence 76^o of the wind direction (in Fig. 2-left, the zone in light color is a leeward zone), the unsteady pressure field applied to the roof structure has been measured with 720 pressure taps, from which $m_{\exp} = 348$ differential unsteady pressures $\mathbb{P}_1^{\exp}(t), \ldots, \mathbb{P}_{m_{\exp}}^{\exp}(t)$ between the interior and exterior locations on the roof have been processed, as well as the associated controllability matrix $[A_c]$. The total duration (brought down to scale 1) of the wind tunnel measurements is $T_{\text{tot}} \simeq 8{,}900$ s. A brief analysis has been carried out to optimize the choice of the number n_p of time steps in the time window for the following reasons. When n_p varies from 256 to 2,048, the number of experimental realizations n_r goes from 96 to 12. The compromise that has been found for choosing n_r and n_p has been based on the following criteria. The number of experimental realizations n_r must be chosen in order to correctly estimate the coefficients of the PCE of $\{\mathbf{P}(t), t \in [0\,, T]\}$. The number of time steps n_p in the time window must be chosen in order that the duration T be large enough for obtaining a sufficiently stationary signal on T and also for obtaining a good frequency resolution. The value $n_p = 1{,}024$ has therefore been retained, which gives $n_r = 24$. From the point of view of signal processing concerning stationarity and statistical estimates of extreme values, it would have been better if the experimental data basis had allow for choosing $n_p = 2{,}048$ and $n_r = 100$, what would lead us to multiplying by 8 the time duration of wind tunnel tests. Finally, the retained values for the signal processing parameters are: $\nu_c = 1.38$ Hz, $\Delta t = 0.36$ s, $T = 371$ s, $n_r = 24$, and $n_p = 1{,}024$. For j equal to 140, 141, 144, and 146, that correspond to pressure taps located in the observed zone, the graphs of the estimate of the power spectral density (PSD) function $f \mapsto S_{P_j^{\exp}}(2\pi f)$ of the experimental centered unsteady pressure $P_j^{\exp}$ is shown in Fig. 3.

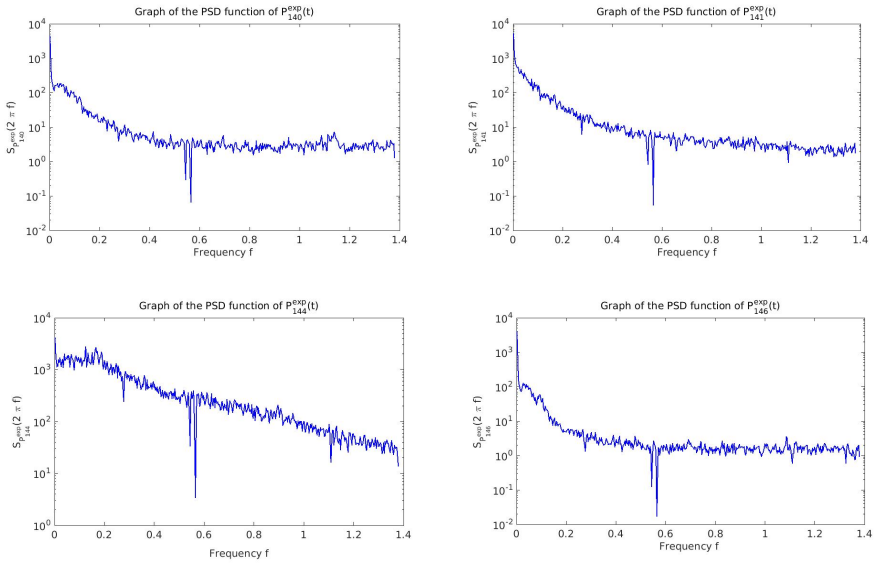

Fig. 3 Graph of the PSD function $f \mapsto S_{P_j^{\exp}}(2\pi f)$ of the experimental $P_j^{\exp}(t)$ for $j = 140, 141, 144, 146$. Horizontal axis in Hz and vertical axis in $\mathrm{N}^2 \times \mathrm{m}^{-4} \times \mathrm{s}$.

In these figures, the small fluctuations that can be seen are due to the relatively small value of n_r. The discontinuities that occur in the vicinity of 0.55 Hz result from processing that has been done on the experimental signals in order to eliminate the peaks corresponding to the harmonics that have been generated by the fan noise.

7.3 Construction of the reduced-order model with the quasi-static acceleration term

Let $\omega \mapsto [\widehat{\mathbb{h}}_N^{c,\mathrm{acc}}(\omega)] = [\mathscr{S}_N^c] + [\varphi_N]\,[\widehat{h}_N(\omega)]\,[\phi_N^c]$ the frequency response function of the linear filter with input $\mathbf{P}$ and output $\mathbf{X}$ defined by Eqs. (2) and (3). A convergence analysis with respect to N of the ROM has been performed by studying the graph of function $N \mapsto \mathrm{conv}(N) = (\int_{\mathscr{B}} \|\widehat{\mathbb{h}}_N^{c,\mathrm{acc}}(\omega)\|_M^2 d\omega)^{1/2}$ with $\|\widehat{\mathbb{h}}_N^{c,\mathrm{acc}}(\omega)\|_M^2 = \mathrm{tr}\{[\widehat{\mathbb{h}}^{c,\mathrm{acc}}(\omega)]^*\,[M]\,[\widehat{\mathbb{h}}^{c,\mathrm{acc}}(\omega)]\}$ in which $[M]$ is the mass matrix of the FE model. For $N = 1$ to 20, Fig. 4 (left) shows the graph of $N \mapsto \mathrm{conv}(N)$. It can be seen that the convergence of the ROM is effectively reached for $N = 12$ and thanks to the presence of the quasi-static acceleration term, the structural modes of ranks larger than 12 are not necessary. Fig. 4 (right) shows the graph of function $f \mapsto \|\widehat{\mathbb{h}}_N^{c,\mathrm{acc}}(2\pi f)\|_M^2$ for $N = 12$.

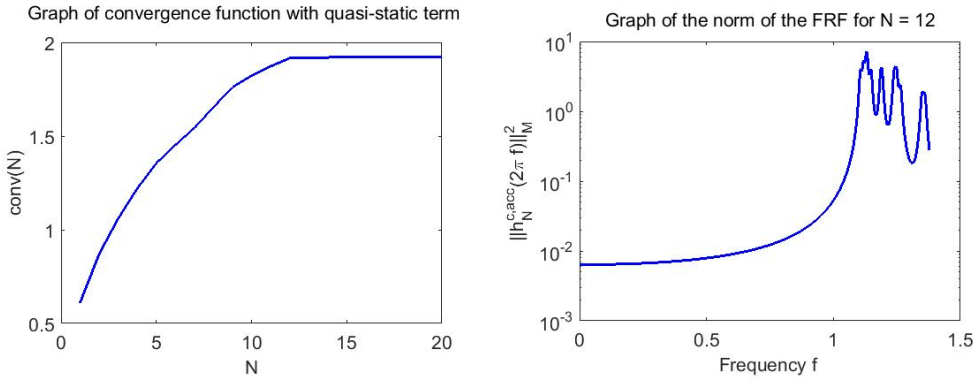

Fig. 4 Graph of function $N \mapsto \mathrm{conv}(N)$ (left) and graph of function $f \mapsto \|\widehat{\mathbb{h}}_N^{c,\mathrm{acc}}(2\pi f)\|_M^2$ for $N = 12$ (right).

*7.4 Generation of additional realizations for non-Gaussian process **P***

The KL statistical reduction of pressure field $\mathbf{P} = \{\mathbf{P}(t), t \in [0,T]\}$ is carried out by using the $n_r = 24$ experimental realizations. As $n_r = 24$, the eigenvalues of the covariance operator of $\mathbf{P}$, for which the ranks are larger than 24 are zero. As 24 is a relatively small value, it is not necessary to envisage a smaller value than 24 and consequently, $N_{\mathrm{KL}} = 24$ is retained. The PCE of random vector $\mathbf{\Gamma}$ is constructed by using the methodology presented in Section 3. For the stochastic computation and the construction of the equivalent static wind loads, $\nu = 1{,}000$ independent realizations of non-Gaussian process $\mathbf{P}$ have been generated by using the generator presented in Section 3. Fig. 5 shows the simulated centered unsteady pressure P_j for $j = 140$ and $j = 141$ in a time window $[0\,, T]$.

7.5 Probability density functions and power spectral density functions of observations

In order to illustrate the type of the numerical results obtained, we present below some probability density functions (PDF) and some power spectral density (PSD) functions of observations. For $\nu =$

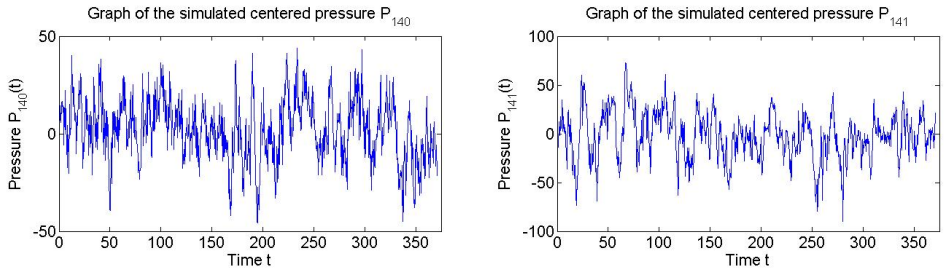

Fig. 5 Graph of the simulated centered unsteady pressure P_j for $j = 140$ and $j = 141$ as a function of time t. Horizontal axis in s and vertical axis in Pa.

1,000 and for $i = 144, 145, 146, 147$, Fig. 6 shows the PDF of $U^i(T)$, of $U^i_{\max} = \max_{t\in[0\,,T]} U^i(t)$, and of $U^i_{\min} = \min_{t\in[0\,,T]} U^i(t)$. The non perfect symmetry of these PDFs is due to the non-Gaussian nature of the observations. It should be noted that these PDF are not perfectly regular due to the chosen number of realizations $\nu = 1{,}000$ (more regular PDF could be obtained in increasing ν using the non-Gaussian generator). Fig. 7 shows the PSD function $f \mapsto S_{U^i}(2\pi f)$ of centered observation U^i. These figures show that there is an important quasi-static contribution in the frequency band $[0\,,0.30]$ Hz.

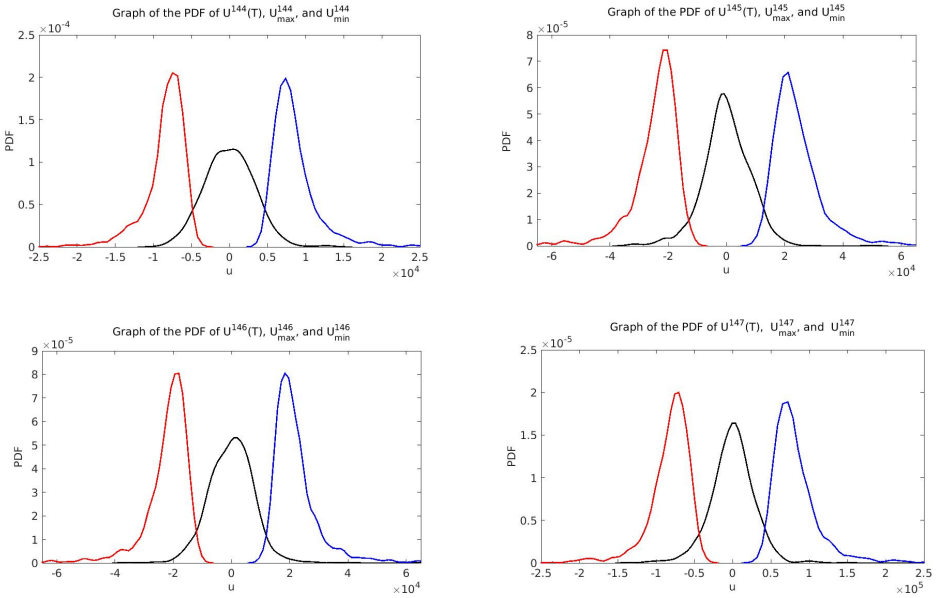

Fig. 6 For $i = 144, 145, 146, 147$, graphs of the PDF of $U^i(T)$ (black line, central curve), $U^i_{\max}$ (blue line, right curve), and $U^i_{\min}$ (red line, left curve). Horizontal axis in Newton (N).

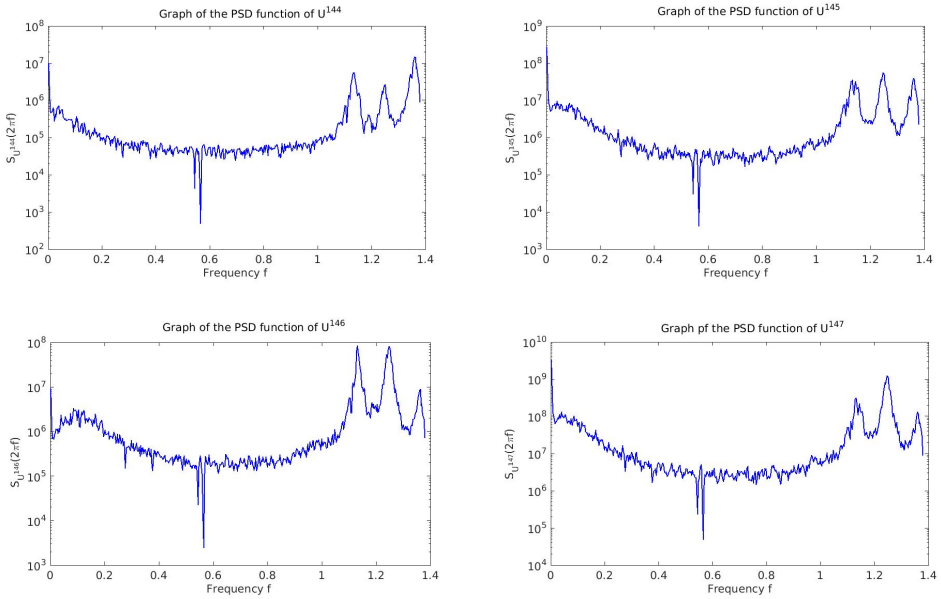

Fig. 7 For $i = 144, 145, 146, 147$, graph of the PSD function $f \mapsto S_{U^i}(2\pi f)$ of centered observation process U^i. Horizontal axis in Hz and vertical axis in $\mathrm{N}^2\times\mathrm{s}$.

7.6 Equivalent static wind loads

7.6.1 Estimation of the equivalent static wind loads

By way of illustration, the presentation of the estimate of ESWL is limited to observation $\mathbb{U}^{144}$. Fig. 8 displays the 2 graphs of 2 components ($y-$force and $z-$force components) of the ESWL.

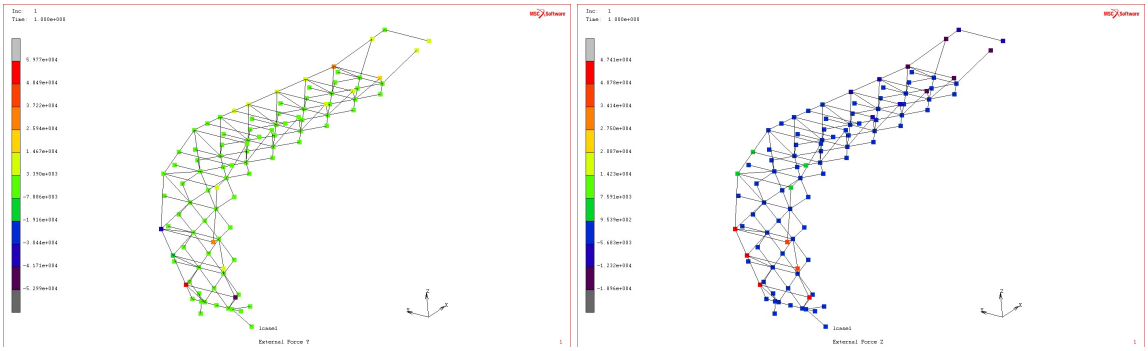

Fig. 8 Graph of each one of 2 components of the ESWL associated with observation $\mathbb{U}^{144}$ at each node of the structure mesh. Vertical axis is in Newton (N).

The dimension of the principal static wind load has been computed and has been found as 37 that is smaller than $m_{\mathbb{f}} = 181$.

Table 1 Numerical values related to $\mathbb{u}^{i,e,s}$ for $i = 144, 145, 146, 147$.

Observation	$\underline{u}^i$	$\underline{\mathbb{U}}^i_{\max}$	$\mathscr{D}^i_{\inf}$	$\mathbb{u}^{i,e,s}$
$\mathbb{U}^{144}$ ($10^4\times$ N)	0.1715	1.031	1.031	1.031
$\mathbb{U}^{145}$ ($10^4\times$ N)	0.8324	3.298	3.298	3.298
$\mathbb{U}^{146}$ ($10^4\times$ N)	0.1740	2.395	2.395	2.395
$\mathbb{U}^{147}$ ($10^4\times$ N)	0.2993	11.30	11.30	11.30

7.6.2 Validation of the approach used for estimating the ESWL

The approach proposed for computing the ESWL can be validated in recomputing the static response of the structure submitted to the ESWL and in comparing the equivalent static observations $\mathbb{u}^{e,s}$ computed with the extreme value statistics of the observation considered. The equivalent static observation $\mathbb{u}^{e,s}$ is given by $\mathbb{u}^{e,s} = [A_o]\,\mathbf{y}^{e,s}$ in which $\mathbf{y}^{e,s}$ is the equivalent static displacement such that $[K]\,\mathbf{y}^{e,s} = \mathbb{f}^{e,s}$. For $i = 144, 145, 146, 147$, the mean value $\underline{u}^i$ is positive. Therefore, for these observations, the worst case corresponds to a maximum. Let $\mathbb{u}^{i,e,s}$ be the equivalent static observation $\mathbb{u}^{e,s}$ associated with $\mathbb{U}^i$, which is such that $\mathbb{u}^{i,e,s} = \underline{u}^i + u^{i,e,s}$. Let $\underline{\mathbb{U}}^i_{\max} = E\{\mathbb{U}^i_{\max}\}$ with $\mathbb{U}^i_{\max} = \max_{t\in[0\,,T]} \mathbb{U}^i(t)$. Let $\mathscr{D}^i_{\inf}$ be the lower bound of the domain associated with $\mathbb{U}^i$. The numerical values obtained are given in Table 1. In Table 1, it can be seen that $\mathbb{u}^{i,e,s}$ is effectively equal to $\underline{\mathbb{U}}^i_{\min}$ for $i = 144, 145, 146, 147$ and consequently, the computation of the ESWL is validated for the domain $\mathscr{D}^i$ that has been used. Note that the optimizer finds the mean $\underline{\mathbb{U}}^i_{\min}$ as an optimal value because the chosen lower bound is $\mathscr{D}^i_{\inf} = \underline{\mathbb{U}}^i_{\max}$ and the probability density function for which the maximum likelihood is searched, presents its maximum for a value slightly higher than $\mathscr{D}^i_{\inf}$, because of the dissymmetry of the non-Gaussian probability density function.

7.7 Gust loading factors

In this method, the gust loading factors are not used for estimating the extreme value statistics of the responses and for the computation of the ESWL. Nevertheless, it is interesting to postprocess the observation stochastic processes in order to compute their gust loading factors. Such a computation allows for comparing the method proposed with the other methods that are based on the Gaussian gust loading factors that are explicitly used for computing the extreme value statistics and for estimating the ESWL. For observation $\mathbb{U}^i$ with $i = 144, 145, 146, 147$, Table 2 presents the gust loading factor g_{gauss} computed with the usual Gaussian hypothesis (see for instance (Davenport 1967)), and the gust loading factors g^+ and g^- postprocessed with the extreme value statistics of each observation estimated with the methodology presented in this paper. The analysis of the results given in this table shows that the values of g_{gauss} are different from the values of g^+ and g^-. This difference comes from the fact that the probability distribution of the extreme values used for computing g_{gauss} is an asymptotic expression based on a Poissonian distribution hypothesis of the point process of upcrossings by high levels (level goes to infinity), the mean value of the upcrossings being calculated with the Rice formula for a Gaussian stochastic process (see Krée and Soize (1986) pp. 136). This expression gives an overestimation of the gust loading factor with respect to the statistical estimation of the extreme value statistics constructed from the non-Gaussian realizations. Note that the gust loading factors are not the same for all the observations what was expected because the responses

depend, simultaneously, on the quasi-static response and on dynamical response related to the 12 modes used in the ROM.

Table 2 Gust loading factors of $\mathbb{U}^i$ for $i = 144, 145, 146, 147$.

Observation	g_{gauss}	g^+	g^-
$\mathbb{U}^{144}$	3.629	2.669	2.674
$\mathbb{U}^{145}$	3.583	3.036	3.015
$\mathbb{U}^{146}$	3.621	2.829	2.831
$\mathbb{U}^{144}$	3.582	2.803	2.796

8. Conclusion

In this paper, we have proposed a novel approach for estimating the equivalent static wind loads for complex structures for which the unsteady pressures are measured in wind tunnel. This approach makes it possible to get rid of restrictive hypotheses and approximations that are often used. This approach also allows a direct assimilation of the experimental data. The method has been validated on a tall building and on a stadium roof for which unsteady pressure measurements were performed. The results obtained show that the prediction lead us to equivalent static forces that are less than those estimated with the usual methods. This approach seems promising and, most certainly, requires further evaluation by applying it to divers situations that fall within the scope of the configurations concerned.

With respect to the existing methods, the novelties of the proposed approach are as follows. (1) The non-Gaussianity of the unsteady pressure field has been taken into account for estimating the extreme values statistics of the time responses. The non-Gaussian character of process **P** has not been described by a given prior probability model for which its hyperparameters would have been identified with the experiments. Non-Gaussian process **P** has been constructed by using a general stochastic model. Consequently, absolutely no hypotheses have been introduced *a priori* and, in addition, not only the non-Gaussian marginal probability distribution of order 1 has been taken into account, but also all the system of the non-Gaussian probability distributions of process **P** has been constructed. (2) This non-Gaussian probability model of process **P** has been used for generating a large number of additional realizations that are required for estimating extreme values statistics of the non-Gaussian time responses. (3) For three-dimensional structures, for which numerous local elastic modes that are outside the frequency band of analysis must be taken into account for ensuring a good convergence of the observations computed with the reduced-order model (ROM), a quasi-static acceleration term has been introduced in the construction of the reduced-order model, which allows for limiting the number of elastic modes to those whose eigenfrequencies belong to the frequency band of analysis while ensuring a perfect convergence of the ROM. (4) A set of observations has been defined, which corresponds to a set of internal forces and/or displacements in given finite elements of the computational model. For each given subset of the set of the observations, an ESWL has been estimated. The principal static wind loads have therefore been classically deduced of the set of the ESWL. (5) For each given subset of observations, the extreme value statistics of the time responses have directly been estimated from the realizations of the responses for which the number of realizations can arbitrarily be large due to the existence of the generator of the non-Gaussian

process **P**, which has been developed. The gust loading factors have thus been deduced from these extreme value statistics, but their values have not been used for estimating the ESWL. (6) A novel approach has been proposed for estimating the ESWL associated with a subset of observations and has been based on the use of a maximum probability principle applied to an adapted random vector of the formulation conditioned by the observation. This approach ensures to preserve the phases of time responses for all the components of the observations subset and avoids the use of classical methods based on the responses envelopes that generally yields an overestimate of the ESWL.

Finally, since no hypotheses have been made on the probability distribution of random pressures, the proposed method can be applied without any conditions on the nature of the probability distribution of the input pressures (probability distribution can be Gaussian or non-Gaussian).

9. Acknowledgment

The authors thank the company ELIOTH of group EGIS for the finite element computational model of the Allianz Riviera stadium in Nice (France).

References

Andrews, H. and Patterson, C. (1976), "Singular value decomposition and digital image processing", *Transactions on Acoustics, Speech, and Signal Processing - IEEE*, **24**(1), 26–53.

Bienkiewicz, B. Tamura, Y. Ham, H.J. Ueda, H. and Hibi, K. (1995), "Proper orthogonal decomposition and reconstruction of multi-channel roof pressure", *Journal of Wind Engineering and Industrial Aerodynamics*, **54**, 369–381.

Biétry, J. Simiu, E. and Sacré, C. (1978), "Mean wind profiles and charge of terrain roughness", *Journal of the Structural Division-ASCE*, **104**(10), 1585–1593.

Biétry, J. Delaunay, D. and Conti, E. (1995), "Comparison of full-scale measurement and computation of wind effects on a cable-stayed bridge", *Journal of Wind Engineering and Industrial Aerodynamics*, **57**(2-3), 225–235.

Blaise, N. and Denoël, V. (2013), "Principal static wind loads", *Journal of Wind Engineering and Industrial Aerodynamics*, **113**, 29-39.

Blaise, N. and Denoël, V. (2015), "Adjusted equivalent static wind loads for non-gaussian linear static analysis", *14th International Conference on Wind Engineering*, Porto Alegre, Brazil, June 21-26.

Blaise, N. Canor, T. and Denoël, V. (2016), "Reconstruction of the envelope of non-Gaussian structural responses with principal static wind loads", *Journal of Wind Engineering and Industrial Aerodynamics*, **149**, 59–76.

Byrd, R.H. Hribar, M.E. and Nocedal, J. (1999), "An interior point algorithm for large-scale nonlinear programming", *SIAM Journal on Optimization*, **9**(4), 877–900.

CEBTP (Center for Research and Studies for Buildings and Public Works) (1978), "Effets du vent sur la Tour Maine-Montparnasse", 15 June. Comlpementary report 1st October 1978.

Chen, X. and Kareem, A. (2004), "Equivalent static wind loads on buildings : New model", *Journal of Structural Engineering*, **130**(10), 1425–1435.

Chen, X. and Zhou, N. (2007), "Equivalent static wind loads on low-rise buildings based on full-scale pressure measurements", *Engineering Structures*, **29**(10), 2563–2575.

Cook, N.J. and Mayne, J.R. (1979), "A novel working approach to the assessment of wind loads for equivalent

static design", *Journal of Wind Engineering and Industrial Aerodynamics*, **4**(2), 149–164.

Davenport, A.G. (1961), "The application of statistical concepts of the wind loading of structures", *Proceeding of the Institution of Civil Engineers*, **19**(4), 449–472.

Davenport, A.G. (1967), "Gust loading factors", *Journal of Structural Division - ASCE*, **93**(3), 11–34.

Davenport A.G. (1995), "How can we simplify and generalize wind loads?", *Journal of Wind Engineering and Industrial Aerodynamics*, **54**, 657-669.

Desceliers, C. Ghanem, R. and Soize, C. (2006), "Maximum likelihood estimation of stochastic chaos representations from experimental data", *International Journal of Numerical Methods in Engineering*, **66**(6), 978–1001.

Ellingwood, B.R. and Tekie, P.B. (1999), "Wind load statistics for probability-based structural design", *Journal of Structural Engineering - ASCE*, **46**(2), 453–463.

Flamand, O. De Oliveira, F. Stathopoulos-Vlamis, A. and Papanikolas, P. (2014), "Conditions for occurrence of vortex shedding on a large cable stayed bridge: Full scale data from monitoring system", *Journal of Wind Engineering and Industrial Aerodynamics*, **135**, 163–169.

Fu, J. Xie, Z. and Li, Q.S. (2010), "Closure to equivalent static wind loads on long-span roof structures", *Journal of Structural Engineering - ASCE*, **136**(4), 470–471.

Ghanem, R. and Spanos, P.D. (1991), *Stochastic Finite Elements: a Spectral Approach*, pringer-Verlag, New York. See also the revised edition (2003), Dover Publications, New York.

Gill, P.E. Murray, W. and Wright, M.H. (1981), *Practical Optimization*, Academic Press, London.

Givens, G.H. and Hoeting, J.A. (2013), *Computational Statistics*, (2nd edition), Wiley, New York.

Golub, G.H. and Van Loan, C.F. (2013), *Matrix Computations*, (4th edition), The Johns Hopkins University Press, Baltimore.

Gu, M. and Huang, Y. (2015), "Equivalent static wind loads for stability design of large span roof structures", *Wind and Structures*, **20**(1), 95–115.

Hillewaere, J. Degroote, J. Lombaert, G. Vierendeels, J. and Degrande, G. (2013), "Computational aspects of simulating wind induced ovalling vibrations in silo groups", *Journal of Computational and Applied Mathematics*, **246**, 161–173.

Hillewaere, J. Degroote, J. Lombaert, G. Vierendeels, J. and Degrande, G. (2015), "Wind-structure interaction simulations of ovalling vibrations in silo groups", *Journal of Fluids and Structures*, **59**, 328–350.

Holmes, J.D. (1992), "Optimised peak load distributions", *Journal of Wind Engineering and Industrial Aerodynamics*, **41**(1-3), 267–276.

Holmes, J.D. (2002), "Effective static load distributions in wind engineering", *Journal of Wind Engineering and Industrial Aerodynamics*, **90**(2), 91–109.

Huang, G. and Chen, X. (2007), "Wind load effects and equivalent static wind loads of tall buildings based on synchronous pressure measurements", *Engineering Structures*, **29**(10), 2641–2653.

Irwin, P.A. (2009), "Wind engineering challenges of the new generation of super-tall buildings", *Journal of Wind Engineering and Industrial Aerodynamics*, **97**(7), 328–334.

Kareem A (1992), "Dynamic response of high-rise buildings to stochastic wind loads", *Journal of Wind Engineering and Industrial Aerodynamics*, **42**(1-3), 1101-1112.

Kasperski, M. and Niemann, H.J. (1988), "On the correlation of dynamic wind loads and structural response of natural-draught cooling towers", *Journal of Wind Engineering and Industrial Aerodynamics*, **30**(1-3), 67–75.

Kasperski, M. (1992), "Extreme wind load distributions for linear and nonlinear design", *Engineering Struc-*

ture, **14**(1), 27–34.

Kasperski, M. and Niemann, H.J. (1992), "The L.R.C (load-response-correlation)-Method. A General Method of Estimating Unfavourable Wind Load. Distributions for Linear and Non-linear Structural Behaviour", *Journal of Wind Engineering and Industrial Aerodynamics*, **43**(1-3), 1753–1763.

Kassir, W. (2017), *A non-Gaussian probabilistic approach for the equivalent static loads of wind effects in structural dynamics from wind tunnel measurements*, Doctoral thesis, Université Paris-Est, France, September 7, 2017.

Kassir, W. Soize, C. Heck, J.V. and De Oliveira F. (2017), "A non-Gaussian probabilistic approach for estimating the equivalent static wind loads on structures from unsteady pressure field", *7th European-African Conference on Wind Engineering*, Lige, Belgium, 4-7 July 2017.

Katsumara, A. Tamura, Y. and Nakamura, O. (2007), "Universal wind load distribution simultaneously reproducing largest load effects in all subject members on large-span cantilevered roof", *Journal of Wind Engineering and Industrial Aerodynamics*, **95**(9), 1145–1165.

Krée, P. and Soize C. (1986), *Mathematics of Random Phenomena*, Reidel, New York. French version: Mécanique Aléatoire, Dunod, Paris, 1983

Kumar, K.S. and Stathopoulos, T. (2000), "Wind loads on low building roofs: A stochastic perspective", *Journal of Structural Engineering - ASCE*, **126**(8), 944–956.

Liang, S.G. Zou, L.H. Wang, D.H. and Huang, G.Q. (2014), "Analysis of three dimensional equivalent static wind loads of symmetric high-rise buildings based on wind tunnel tests", *Wind and Structures*, **19**(5), 565–583.

Lou, W. Zhang, L. Huang, M.F. and Li, Q.S. (2015), "Multiobjective equivalent static wind loads on complex tall buildings using non-Gaussian peak factors", *Journal of Structural Engineering*, **141**(11), 04015033.

Lu, C.L. Huang, S.H. Tuan, A.Y. Zhi, L.H. and Su, S. (2016), "Evaluation of wind loads and wind induced responses of a super-tall building by large eddy simulation", *Wind and Structures*, **23**(4), 313–350.

Ohayon, R. and Soize, C. (1998), *Structural Acoustic and Vibration*, Academic Press, San Diego, London.

Patruno, L. Ricci, M. de Miranda, S. and Ubertini, F. (2017), "An efficient approach to the determination of Equivalent Static Wind Loads", *Journal of Fluids and Structures*, **68**, 1–14.

Perrin, G. Soize, C. Duhamel, D. and Funfschilling, C. (2012), "Identification of polynomial chaos representations in high dimension from a set of realizations", *SIAM Journal on Scientific Computing*, **34**(6), A2917–A2945.

Repetto, M.P. and Solari, G. (2004), "Equivalent static wind actions on vertical structures", *Journal of Wind Engineering and Industrial Aerodynamics*, **92**(5), 335–357.

Simiu, E. and Scanlan, R.H. (1996), *Wind Effects on Structures. Fundamentals and Applications to Design*, (3rd edition), John Wiley & Sons, New York.

Simiu, E. (2015), "Equivalent static wind loads for tall building design", *Journal of the Structural Division - ASCE*, **102**(4), 719–737.

Soize, C. (1978), "Gust loading factors with nonlinear pressure terms", *Journal of the Structural Division - ASCE*, **104**(6), 991–1007.

Soize, C. (2017), *Uncertainty quantification. An Accelerated Course with Advanced Applications in Computational Engineering*, Springer, New York.

Solari, G. (1985), "Mathematical model to predict 3-D wind loading on buildings", *Journal of Engineering Mechanics - ASCE*, **111**(2), 254–276.

Solliec, C. and Mary, J. (1995), "Simultaneous measurements of fluctuating pressures using piezoresistive multichannel transducers as applied to atmospheric wind tunnel tests", *Journal of Wind Engineering and*

Industrial Aerodynamics, **56**(1), 71–86.

Sun, W. Gu, M. and Zhou, X. (2015), "Universal Equivalent Static Wind Loads of Fluctuating Wind Loads on Large-Span Roofs Based on POD Compensation", *Advances in Structural Engineering*, **18**(9), 1443–1459.

Tamura, Y. Suganuma, S. Kikuchi, H. and Hibi, K. (1999), "Proper Orthogonal Decomposition of Random Wind Pressure Field", *Journal of Fluids and Structures*, **13**(7), 1069–1095.

Uematsu, Y. Yamada, M. Inoue, A. and Hongo, T. (1997), "Wind loads and wind-induced dynamic behavior of a single-layer latticed dome", *Journal of Wind Engineering and Industrial Aerodynamics*, **66**(3), 227–248.

Uematsu, Y. Moteki, T. and Hongo, T. (2008), "Model of wind pressure field on circular flat roofs and its application to load estimation", *Journal of Wind Engineering and Industrial Aerodynamics*, **96**(6), 1003–1014.

Vaicaitis, R. Shinozuka, M. Takeno, M. (1973), "Parametric study of wind loading on structures", *Journal of Structural Division - ASCE*, **99**(3), 453–468.

Vaicaitis, R. and Simiu, E. (1977), "Nonlinear pressure terms and along-wind response", *Journal of the Structural Division - ASCE*, **103**(4), 903–906.

Vickery, B.J. and Danveport, A.G. (1967), "A comparison of theoretical and experimental determination of the response of elastic structures to turbulent flow", *Proceedings of the Second Conference on Wind Effects on Buildings and Structures*, **1**, 705–738, Ottawa, Canada.

Vinet, J. and De Oliveira, F. (2011), "Etudes aérodynamiques de dimensionnement au vent du Stade Vélodrome de Marseille : nouvelles configurations", EN-CAPE 11.114 C V2, CSTB, Nantes, France.

Vinet, J. and De Oliveira, F. (2013), "Etude aérodynamiques de dimensionnement au vent du stade de Nice", EN-CAPE 11.056 C-V1, CSTB, Nantes, France. Rapport confidentiel.

Vinet, J. De Oliveira, F. Barre, C. Fayette, E. Consigny, F. and Vondiere, R. (2015), "Wind effects on stadium refurbishment the example of Stade Velodrome in Marseille, France", *Proceedings of the 14th International Conference on Wind Engineering (ICWE14)*, Porto Alegre, Brazil, June 21-26.

Yang, Q.S. Chen, B. Wu, Y. and Tamura, Y. (2013), "Wind-Induced Response and Equivalent Static Wind Load of Long-Span Roof Structures by Combined Ritz-Proper Orthogonal Decomposition Method", *Journal of Structural Engineering - ASCE*, **139**(6), 997–1008.

Yi, J. Zhang, J.W. and Li, Q.S. (2013), "Dynamic characteristics and wind-induced responses of a super-tall building during typhoons", *Journal of Wind Engineering and Industrial Aerodynamics*, **121**, 116–130.

Zhang, X. and Yao, M. (2015), "Numerical investigation on the wind stability of super long-span partially earth-anchored cable-stayed bridges", *Wind and Structures*, **21**(4), 407–424.

Zhou, Y. Gu, M. and Xiang, H.F. (1999), "Alongwind static equivalent wind loads and responses of tall buildings. Part I: Unfavorable distributions of static equivalent wind loads", *Journal of Wind Engineering and Industrial Aerodynamics*, **79**(1), 135–150.

Zhou, Y. Gu, M. and Xiang, H.F. (1999), "Alongwind static equivalent wind loads and responses of tall buildings. Part II: Effects of mode shapes", *Journal of Wind Engineering and Industrial Aerodynamics*, **79**(1-2), 151–158.

Zhou, X. and Gu, M. (2010), "An approximation method for computing the dynamic responses and equivalent static wind loads of large-span roof structures", *International Journal of Structural Stability and Dynamics*, **10**(5), 1141–1165.

Zhi, L. Li, Q.S. and Fang, M. (2016), "Identification of Wind Loads and Estimation of Structural Responses of Super-Tall Buildings by an Inverse Method", *Computer-Aided Civil and Infrastructure Engineering*, **31**(12), 966–982.